EMBO reports

scientific report

The cellular level of telomere dysfunction determines induction of senescence or apoptosis *in vivo*

André Lechel[1], Ande Satyanarayana[1], Zhenyu Ju[1], Ruben R. Plentz[1], Sonja Schaetzlein[1], Cornelia Rudolph[2], Ludwig Wilkens[2], Stephanie U. Wiemann[1], Gabriele Saretzki[4], Nisar P. Malek[1], Michael P. Manns[1], Jan Buer[3,5] & K. Lenhard Rudolph[1+]

[1]Department of Gastroenterology, Hepatology, and Endocrinology, [2]Institute of Cell and Molecular Pathology, and [3]Institute of Medical Microbiology, Medical School Hannover, Hannover, Germany, [4]Institute for Ageing and Health, University of Newcastle, Newcastle upon Tyne, UK, and [5]Department of Cell Biology, GBF, Braunschweig, Germany

Telomere dysfunction induces two types of cellular response: cellular senescence and apoptosis. We analysed the extent to which the cellular level of telomere dysfunction and *p53* gene status affect these cellular responses in mouse liver using the experimental system of TRF2 inhibition by a dominant-negative version of the protein (TRF2$^{\Delta B \Delta M}$). We show that the level of telomere dysfunction correlates with the level of TRF2$^{\Delta B \Delta M}$ protein expression resulting in chromosomal fusions, aberrant mitotic figures and aneuploidy of liver cells. These alterations provoked *p53*-independent apoptosis, but a strictly *p53*-dependent senescence response in distinct populations of mouse liver cells depending on the cellular level of TRF2$^{\Delta B \Delta M}$ expression. Apoptosis was associated with higher expression of TRF2$^{\Delta B \Delta M}$, whereas cellular senescence was associated with low levels of TRF2$^{\Delta B \Delta M}$ expression. Our data provide experimental evidence that induction of senescence or apoptosis *in vivo* depends on the cellular level of telomere dysfunction and differentially on *p53* gene function.

Keywords: telomere; TRF2; Terc; p53; senescence

EMBO reports (2005) **6**, 275–281. doi:10.1038/sj.embor.7400352

INTRODUCTION

The main function of telomeres is to cap chromosomal ends and thus to prevent chromosomal fusions and activation of DNA damage responses (Blackburn *et al*, 2000; de Lange, 2002). It has been shown that telomere shortening leads to loss of telomere function and induction of DNA-damage responses (Shay *et al*, 1991; Chin *et al*, 1999; Karlseder *et al*, 1999; d'Adda di Fagagna *et al*, 2003; Satyanarayana *et al*, 2004a). *In vitro* experiments have suggested that a two-stage checkpoint response exists in response to different levels of telomere dysfunction (Shay *et al*, 1991). According to this hypothesis, moderate telomere dysfunction induces senescence at the mortality stage 1 (M1). However, if *p53* is lost, cells bypass the senescence checkpoint and continue to proliferate, eventually reaching a second mortality stage (M2) characterized by massive cell death and chromosomal instability (crisis). Whether this model applies to the *in vivo* situation is under debate.

In telomerase-deficient (*Terc*$^{-/-}$) mice, telomere shortening induced two different cellular phenotypes: apoptosis and senescence (Lee *et al*, 1998; Satyanarayana *et al*, 2003). In compound mutant mice lacking *p53* and *Terc*, organ phenotypes induced by telomere dysfunction were rescued. However, these reappeared in a late generation of *Terc*$^{-/-}$ *p53*$^{-/-}$ double-knockout mice, suggesting that *p53*-independent signals can mediate responses to telomere dysfunction *in vivo* (Chin *et al*, 1999).

To analyse the influence of the level of telomere dysfunction on cellular responses *in vivo*, we used the experimental system of TRF2 inhibition, which leads to telomere dysfunction and chromosomal fusions (van Steensel *et al*, 1998). *In vitro* experiments have established that inhibition of TRF2 provokes the same phenotypes as telomere shortening: senescence and apoptosis (Karlseder *et al*, 1999, 2002; Smogorzewska & de Lange, 2002).

In the present study, we analysed the consequences of the loss of telomere protection by TRF2 inhibition in the mouse liver. The cellular responses were analysed in correlation with the level of telomere protection and *p53* gene status. Our study demonstrates that the cellular level of telomere dysfunction determines the type of damage response that occurs and provides experimental evidence that telomere dysfunction provokes both *p53*-dependent and *p53*-independent effects in mouse liver cells.

[1]Department of Gastroenterology, Hepatology, and Endocrinology, [2]Institute of Cell and Molecular Pathology, and [3]Institute of Medical Microbiology, Medical School Hannover, Carl-Neuberg-Strasse 1, 30625 Hannover, Germany
[4]Institute for Ageing and Health, University of Newcastle, Newcastle upon Tyne NE4 6BE, UK
[5]Department of Cell Biology, Gesellschaft für Biotechnologische Forschung, Braunschweig, Germany
[+]Corresponding author. Tel: +49 511 532 6999; Fax: +49 511 532 6998; E-mail: rudolph.lenhard@mh-hannover.de

Received 23 August 2004; revised 21 December 2004; accepted 18 January 2005; published online 18 February 2005

RESULTS

Dose-dependent induction of telomere dysfunction

We analysed chromosomal fusions, anaphase bridges and ploidy of liver cells in response to adenoviral-mediated TRF2$^{\Delta B\Delta M}$ expression in mouse liver. The level of TRF2$^{\Delta B\Delta M}$ protein expression peaked 24 h after virus application (Fig 1A). Chromosomal fusions were detected at a rate of 1.03 fusions per metaphase 72 h after adenovirus TRF2$^{\Delta B\Delta M}$ (Ad TRF2$^{\Delta B\Delta M}$) infection. Chromosomal fusions often contained telomere sequence, and there were high rates of telomere free ends (Fig 1B–F). We did not detect a significant degradation of the telomeric G-strand in mouse liver infected with Ad TRF2$^{\Delta B\Delta M}$ (supplementary Fig 1 online), which is possibly due to the relatively low percentage of TRF2$^{\Delta B\Delta M}$-infected liver cells in our *in vivo* system (supplementary Fig 2 online; also see below and Fig 3F) compared with previous *in vitro* experiments. In our *in vivo* system, the majority of infected liver cells were hepatocytes, as determined on the basis of cell morphology (data not shown).

Ad TRF2$^{\Delta B\Delta M}$-infected mouse liver showed high rates of aberrant mitosis (Fig 1G), including misaligned metaphase chromosomes, triphasic spindles, and most importantly, frequent anaphase bridges (Fig 1H,I). The prevalence of higher rates of mitotic figures in Ad TRF2$^{\Delta B\Delta M}$-infected mice compared with control mice was in line with previous observations showing that telomere dysfunction induces a delay in mitosis progression, thus increasing the rate of mitotic figures in regenerating liver (Rudolph *et al*, 2000). Telomere dysfunction and aberrant mitosis resulted in severe polyploidy of liver cells in TRF2$^{\Delta B\Delta M}$-infected mice (supplementary Fig 3 online). Adenovirus (Ad) green fluorescent protein (GFP)-infected control mice did not show telomere dysfunction, anaphase bridges or polyploidy (Fig 1G; supplementary Fig 3 online). The analysis of aberrant mitosis and anaphase bridges in mouse liver after application of different doses of Ad TRF2$^{\Delta B\Delta M}$ showed a strong correlation between the level of Ad TRF2$^{\Delta B\Delta M}$ infection and induction of aberrant mitosis (Fig 1J).

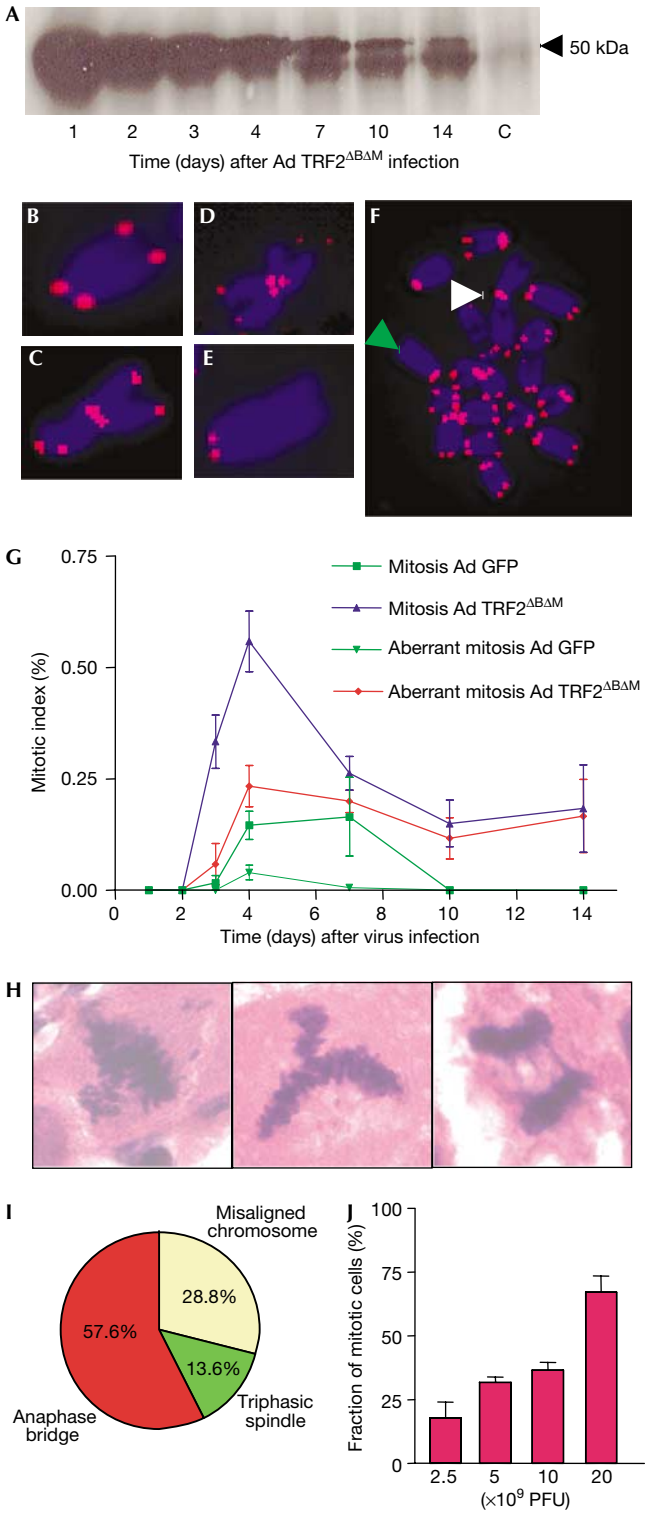

Fig 1 | TRF2$^{\Delta B\Delta M}$ induces telomere dysfunction in mouse liver. Mice were injected intravenously with Ad TRF2$^{\Delta B\Delta M}$ (1×10^{10} PFU/ml) or with control Ad GFP (1×10^{10} PFU/ml, $n = 21$ mice per group, three mice per time point). (**A**) Protein expression level of TRF2$^{\Delta B\Delta M}$ in protein extracts (100 μg) from whole-cell lysates of mouse liver. (**B–F**) Representative photographs of metaphase chromosomes from mouse liver cells, 72 h after Ad TRF2$^{\Delta B\Delta M}$ (1×10^{10} PFU/ml) infection. A telomere-specific probe was used for fluorescence *in situ* hybridization (FISH; counter staining: DAPI). (**B**) Normal chromosome with telomere signal on either side of chromosome arms. (**C**) Fusion involving both p-arms of the fused chromosomes with telomeric sequence at the fusion point. (**D**) Single short-arm chromatid fusion involving only one p-arm with telomeric sequence at the fusion point. (**E**) Telomere free end at the q-arm of the chromosome. (**F**) Metaphase: the white arrowhead shows chromosomal fusion, and the green arrowhead points to telomere-free end. (**G**) Graph of the rate of aberrant mitosis at the indicated time points after virus infection. The rate of aberrant mitosis was significantly higher in the liver of Ad TRF2$^{\Delta B\Delta M}$-infected mice compared with Ad GFP-infected mice (e.g. rate of aberrant mitosis at day 4 after virus infection: 0.233 ± 0.033 in Ad TRF2$^{\Delta B\Delta M}$-infected mice versus 0.040 ± 0.033 in Ad GFP-infected mice, $P = 0.006$). (**H**) Representative photographs and (**I**) piechart of the types of aberrant mitotic figure observed in Ad TRF2$^{\Delta B\Delta M}$-infected mouse liver. (**H**) From left to right: misaligned chromosome, triphasic spindle and anaphase bridge (magnification: × 1,000). (**J**) Percentage of aberrant mitotic figures 120 h after Ad TRF2$^{\Delta B\Delta M}$ infection at different viral concentrations.

Induction of apoptosis and senescence

TRF2$^{\Delta B\Delta M}$ adenovirus produced an apoptotic response peaking at 48–72 h after virus application, which was not seen in Ad GFP-infected control mice (Fig 2A,B). At later time points (day 7 after virus infection), Ad TRF2$^{\Delta B\Delta M}$-infected mouse liver no longer showed elevated rates of apoptosis compared with Ad GFP-infected control mouse liver. Senescence-associated β-galactosidase (SA-β-Gal)-positive liver cells were detected first at 48 h after adenoviral delivery of TRF2$^{\Delta B\Delta M}$ but not in Ad GFP-infected control mice (Fig 2C,D).

Outcome – dependent on level of mutant TRF2

Co-staining of SA-β-Gal and TUNEL showed that senescence and apoptosis were induced in different populations of mouse liver cells in response to TRF2$^{\Delta B\Delta M}$ infection (Fig 3A–C). Co-staining of TUNEL, SA-β-Gal and TRF2$^{\Delta B\Delta M}$ showed that apoptotic cells showed stronger staining for TRF2$^{\Delta B\Delta M}$, whereas SA-β-Gal-positive liver showed weaker staining for TRF2$^{\Delta B\Delta M}$ (supplementary Fig 4A–C online). After infection of mice with different titres of Ad TRF2$^{\Delta B\Delta M}$, a strong dose–response correlation between the titre of TRF2$^{\Delta B\Delta M}$ infection and the rate of apoptotic liver cells was observed at day 2 after viral infection (Fig 3D). In contrast to the apoptotic response, the induction of SA-β-Gal activity was sustained and showed a slight increase at day 7 after Ad TRF2$^{\Delta B\Delta M}$ infection (Fig 3E). These data correlated with the observation that the percentage of liver cells expressing high levels of TRF2$^{\Delta B\Delta M}$ decreased at day 7 compared with day 2 after virus infection, whereas the percentage of liver cells expressing weak levels of TRF2$^{\Delta B\Delta M}$ increased at the same time interval (Fig 3F). Fluorescence-activated cell sorting (FACS) analysis on liver cell suspension co-stained for TUNEL and TRF2$^{\Delta B\Delta M}$ confirmed a positive correlation between the cellular level of TRF2$^{\Delta B\Delta M}$ expression and apoptosis of liver cells (Fig 3G). To analyse the correlation between senescence and the level of TRF2$^{\Delta B\Delta M}$, cell size was monitored according to previous studies, which have shown a significant increase in cell size of senescent cells, detectable by FACS analysis (Gorbunova *et al*, 2003; Martin-Ruiz *et al*, 2004). This analysis showed an inverse relationship between the cellular level of TRF2$^{\Delta B\Delta M}$ expression and the rate of senescent liver cells (Fig 3H).

Role of *p53* in apoptosis and senescence

To identify the role of *p53* in response to different levels of telomere dysfunction induced by TRF2$^{\Delta B\Delta M}$ in mouse liver cells, we studied induction of apoptosis and senescence in *p53*$^{-/-}$ and *p53*$^{+/+}$ mice 48 h after infection with Ad TRF2$^{\Delta B\Delta M}$ (Fig 4). The rate of apoptosis induced by Ad TRF2$^{\Delta B\Delta M}$ infection was almost identical in *p53*$^{+/+}$ and *p53*$^{-/-}$ mice (Fig 4A,C). In contrast, the induction of senescence by Ad TRF2$^{\Delta B\Delta M}$ infection was markedly reduced in *p53*$^{-/-}$ mice compared with *p53*$^{+/+}$ mice (Fig 4B,D).

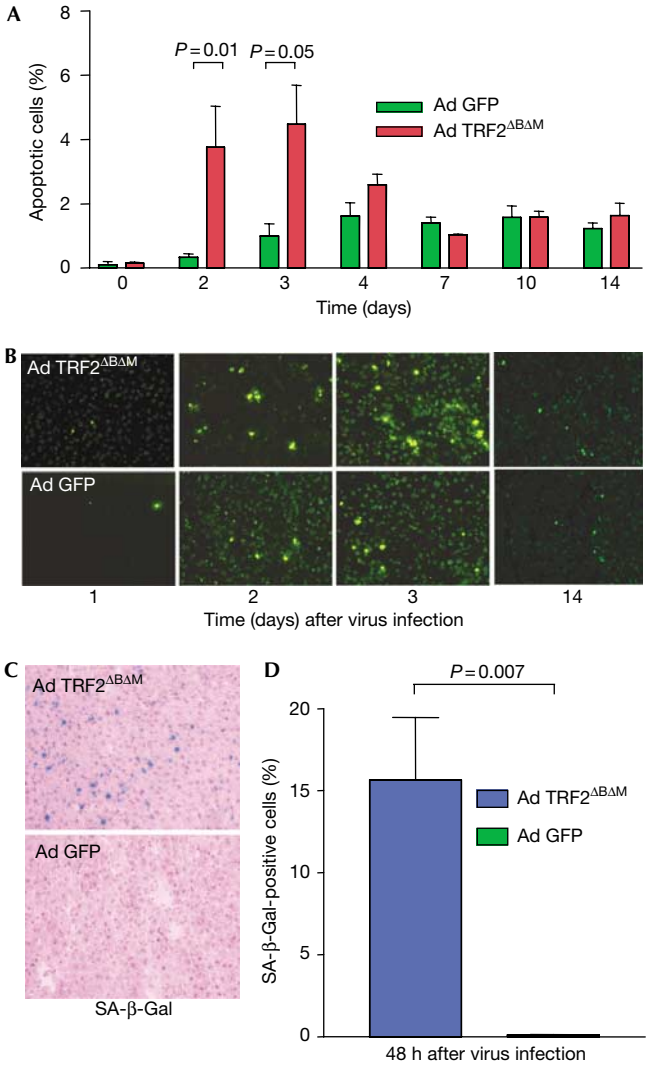

Fig 2 | TRF2$^{\Delta B\Delta M}$ induces apoptosis and senescence in the mouse liver. Apoptosis was determined by TUNEL assay on liver sections from mice infected with Ad TRF2$^{\Delta B\Delta M}$ or Ad GFP (1×10^{10} PFU/ml, $n = 21$ mice per group, $n = 3$ mice per time point). (**A**) Percentage of apoptotic liver cells at the indicated time points. Note that Ad TRF2$^{\Delta B\Delta M}$ induced significantly higher rates of apoptosis compared with Ad GFP-infected mice at early time points when maximal levels of TRF2$^{\Delta B\Delta M}$ were expressed ($P = 0.01$ at day 2 after virus infection; $P = 0.05$ at day 3 after virus infection). (**B**) Representative photographs of apoptotic liver cells as detected by TUNEL assay at the indicated time points after virus infection (magnification: × 200). (**C**) Representative photographs of SA-β-Gal-positive liver cells 48 h after Ad TRF2$^{\Delta B\Delta M}$ (top) and Ad GFP infection (bottom) (magnification: × 200). (**D**) Percentage of liver cells positive for SA-β-Gal staining in Ad TRF2$^{\Delta B\Delta M}$-infected mice compared with Ad GFP-infected mice.

DISCUSSION

Our current study shows that TRF2$^{\Delta B\Delta M}$ expression provokes acute telomere dysfunction, chromosomal fusions, aberrant mitosis and polyploidy in mouse liver cells *in vivo*. One limitation of this experimental system is that it does not mimic the gradual telomere attrition that is observed in physiological processes *in vivo*. Conversely, TRF2 inhibition seems to be a functional surrogate for telomere dysfunction arising from telomere attrition, as shown by its ability to promote anaphase bridging in a dose-dependent manner. This system allowed us to pinpoint specific downstream signalling responses to different levels of telomere dysfunction in the mouse liver.

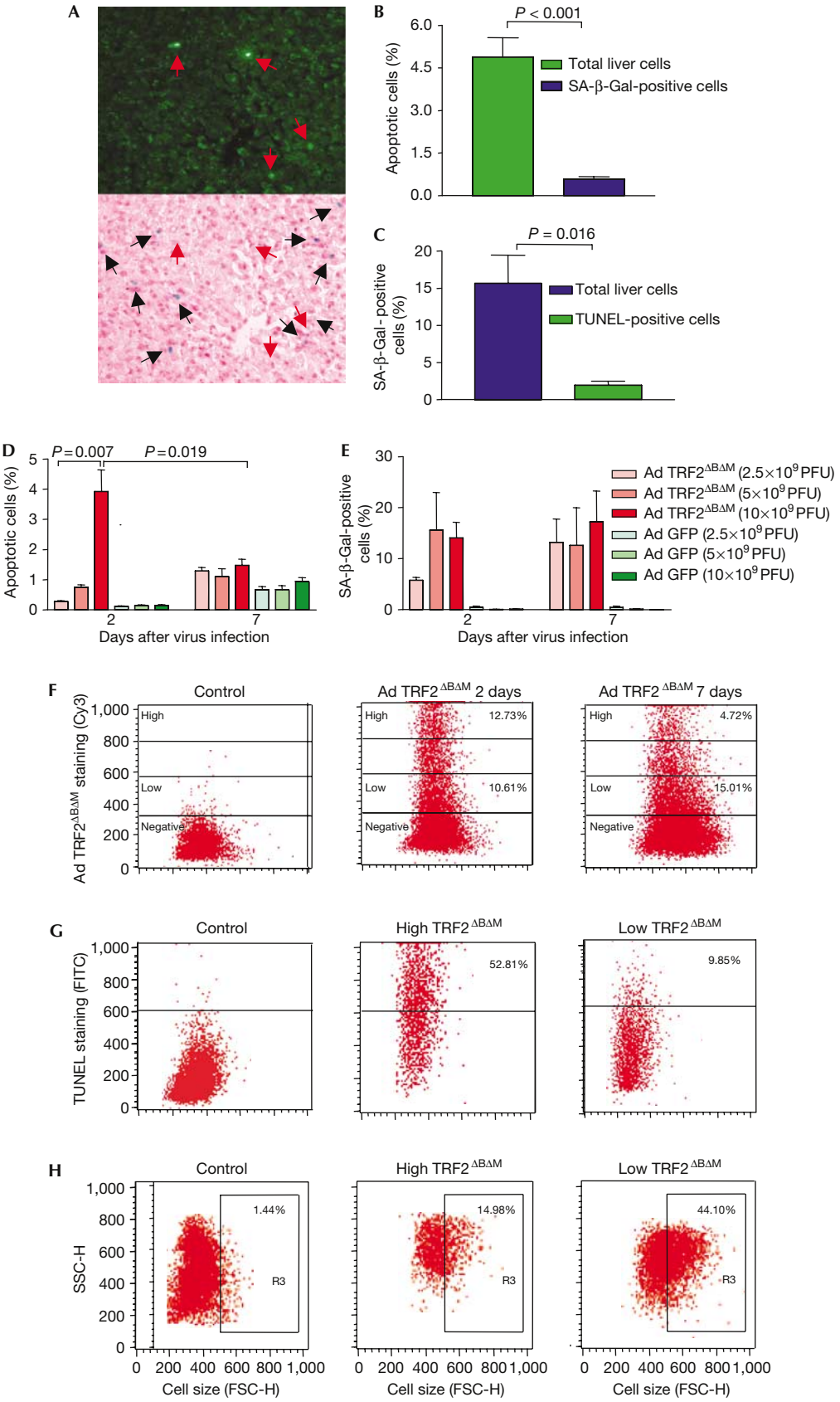

◀ **Fig 3** | Induction of apoptosis or senescence depends on the level of TRF2$^{\Delta B\Delta M}$ expression in mouse liver. The localization of apoptotic and senescent cells was analysed in liver sections of mice infected with Ad TRF2$^{\Delta B\Delta M}$ (1×10^{10} PFU/ml; $n = 4$). (**A**) Representative photographs of TUNEL and SA-β-Gal co-staining. Upper panel: TUNEL staining; lower panel: SA-β-Gal staining with haemotoxylin and eosin counterstaining. Note that the SA-β-Gal-positive cells (black arrows) can be discriminated from the green fluorescent apoptotic liver cells (red arrows) (magnification: ×200). (**B**) Histogram of the prevalence of SA-β-Gal-positive liver cells 48 h after Ad TRF2$^{\Delta B\Delta M}$ infection (1×10^{10} PFU/ml): 15.7% of total liver cells were SA-β-Gal positive, whereas only 1.9% of TUNEL-positive liver cells were SA-β-Gal positive ($P = 0.016$). (**C**) Histogram of the prevalence of apoptotic liver cells 48 h after Ad TRF2$^{\Delta B\Delta M}$ infection (1×10^{10} PFU/ml): 4.9% of total liver cells were TUNEL positive, whereas only 0.6% of SA-β-Gal-positive liver cells were TUNEL positive ($P < 0.001$). (**D**) Dose–response analysis of the percentage of TUNEL-positive cells in correlation with the titre of virus infection. The dose of Ad TRF2$^{\Delta B\Delta M}$ infection correlates with the level of apoptosis at day 2 after virus infection. (**E**) Dose–response analysis of the percentage of SA-β-Gal-positive cells in correlation with the titre of virus infection. There was no significant dose–response correlation. Note that in contrast to the apoptosis response, the rate of SA-β-Gal-positive liver cells increased at day 7 after virus infection. (**F**) Percentage of TRF2$^{\Delta B\Delta M}$-positive liver cells as determined by FACS analysis of liver-cell suspensions at the indicated time points after virus infection (1×10^{10} PFU/ml). Left: Ad GFP-infected control mouse liver; middle: Ad TRF2$^{\Delta B\Delta M}$-infected mouse liver at day 2 after viral infection; right: Ad TRF2$^{\Delta B\Delta M}$-infected mouse liver at day 7 after viral infection. Note the decrease in liver cells expressing a high level of TRF2$^{\Delta B\Delta M}$ but the increase in liver cells expressing a low level of TRF2$^{\Delta B\Delta M}$ at day 7 compared with day 2 after viral infection. (**G**) Representative graphs of the percentage of TUNEL-positive cells in liver-cell suspensions analysed by FACS at day 2 after virus infection (1×10^{10} PFU/ml). Left: control mouse liver; middle: fraction of liver cells expressing high levels of TRF2$^{\Delta B\Delta M}$ (52.8% of the cells stain positive for TUNEL); right: fraction of liver cells expressing low levels of TRF2$^{\Delta B\Delta M}$ (9.85% of the cells stain positive for TUNEL). The gates for the expression level of TRF2$^{\Delta B\Delta M}$ were set according to the labelling in (**F**). (**H**) Representative graphs of the percentage of senescent liver cells as analysed on the basis of cell size by FACS of liver-cell suspension at day 7 after virus infection. The gate R3 contains cells that have an increase in cell size (FSC, increase in forward scatter). Left: control mouse liver; middle: fraction of liver cells expressing high levels of TRF2$^{\Delta B\Delta M}$ (29.1% of the cells show a senescence-associated increase in cell size); right: fraction of liver cells expressing low levels of TRF2$^{\Delta B\Delta M}$ (44.1% of the cells show a senescence-associated increase in cell size). The gates for the expression level of TRF2$^{\Delta B\Delta M}$ were set according to the labelling in (**F**).

Our study shows that the cellular level of the loss of telomere protection dictates the type of damage response induced in liver cells *in vivo*. The data show that senescence induced by low levels of TRF2$^{\Delta B\Delta M}$ expression is *p53* dependent, whereas apoptosis induced by high levels of TRF2$^{\Delta B\Delta M}$ expression is *p53* independent. Our results differ from previous reports, which showed a strict *p53* dependency of apoptosis induced by TRF2$^{\Delta B\Delta M}$ in mouse fibroblasts and human cancer cell lines *in vitro* (Karlseder *et al*, 1999). A possible explanation is that the accumulation of genetic alterations in mouse embryo fibroblasts (Parrinello *et al*, 2003) and human cancer cells alters the cellular responses to telomere dysfunction. Our data suggest that *in vivo* a two-stage checkpoint exists in response to different levels of telomere dysfunction. These data are in agreement with the classical model of two mortality stages of primary human fibroblasts in response to moderate or severe telomere dysfunction (Shay *et al*, 1991). Given that telomere shortening is a property of ageing cells and an early feature of various cancers (Djojosubroto *et al*, 2003; Satyanarayana *et al*, 2004b), it is possible that this two-stage checkpoint response to telomere dysfunction is necessary for tumour suppression *in vivo*. An increase in senescent cells has been demonstrated in various mammalian tissues during ageing (Dimri *et al*, 1995; Krishnamurthy *et al*, 2004). It remains to be analysed how frequently cells bypass the M1 checkpoint of senescence in *vivo* and how this contributes to cancer initiation in aged human tissue.

METHODS

Mice. For this study, we used 12- to 14-week-old female mice in a C57Bl/6J background and, for the *p53*-related experiments, C57Bl/6J-Tr*p53*tm1Tyj.

Western blotting. Proteins subjected to SDS–polyacrylamide gel electrophoresis were detected using antibody against human TRF2 (1:10,000; anti-TRF2 05-521, Upstate, Charlottesville, VA, USA), which recognizes TRF2$^{\Delta B\Delta M}$ but not endogenous mouse TRF2.

G-strand overhang assay. The assay was carried out as described previously (Cimino-Reale *et al*, 2001; Keys *et al*, 2004).

Adenovirus amplification and purification. All viruses were produced in HEK-293 cells and titred at the same time point in the same manner according to standard protocols. To assure a similar rate of adenovirus infection in different areas of mouse liver, the expression level of GFP was monitored 48 h after infection in all five liver lobes of an individual mouse infected with Ad GFP (supplementary Fig 5 online).

Apoptosis staining. The rate of apoptosis was determined by TUNEL assay (*In situ* cell detection kit, Roche, Mannheim, Germany). The number of apoptotic cells was determined in 20 low-power fields (×200) and expressed as a percentage of all cells counted.

Senescence-associated β-galactosidase staining. SA-β-Gal staining was carried out as described previously (Dimri *et al*, 1995). The number of SA-β-Gal-positive cells was determined in 20 randomly chosen low-power fields (×100) and expressed as a percentage of all cells counted.

Apoptosis–SA-β-galactosidase co-staining. The SA-β-Gal-stained sections were permeabilized with 1% Triton X-100 and 0.1% sodium citrate followed by TUNEL staining and counterstaining with DAPI. The number of apoptotic ($n = 422$) and SA-β-Gal-positive cells ($n = 1{,}200$) was analysed randomly in low-power fields (×200) chosen at random ($n = 4$ mice).

SA-β-galactosidase–TRF2 co-staining. The SA-β-Gal-stained sections were permeabilized in 10 mM citric acid–sodium phosphate buffer at 95 °C for 7 min followed by incubation with anti-TRF2 antibody (1:300) for 1 h. The detection was performed by Cy3-labelled rabbit anti-mouse antibody (1:500; Zymed, San Francisco, CA, USA). The number of SA-β-Gal-positive cells ($n = 600$) in correlation with the level of TRF2$^{\Delta B\Delta M}$ expression was counted in randomly chosen low-power fields (×200; $n = 4$ mice).

Apoptosis–TRF2 co-staining. TUNEL-stained slides were incubated with TRF2 antibody (1:300) for 1 h followed by incubation

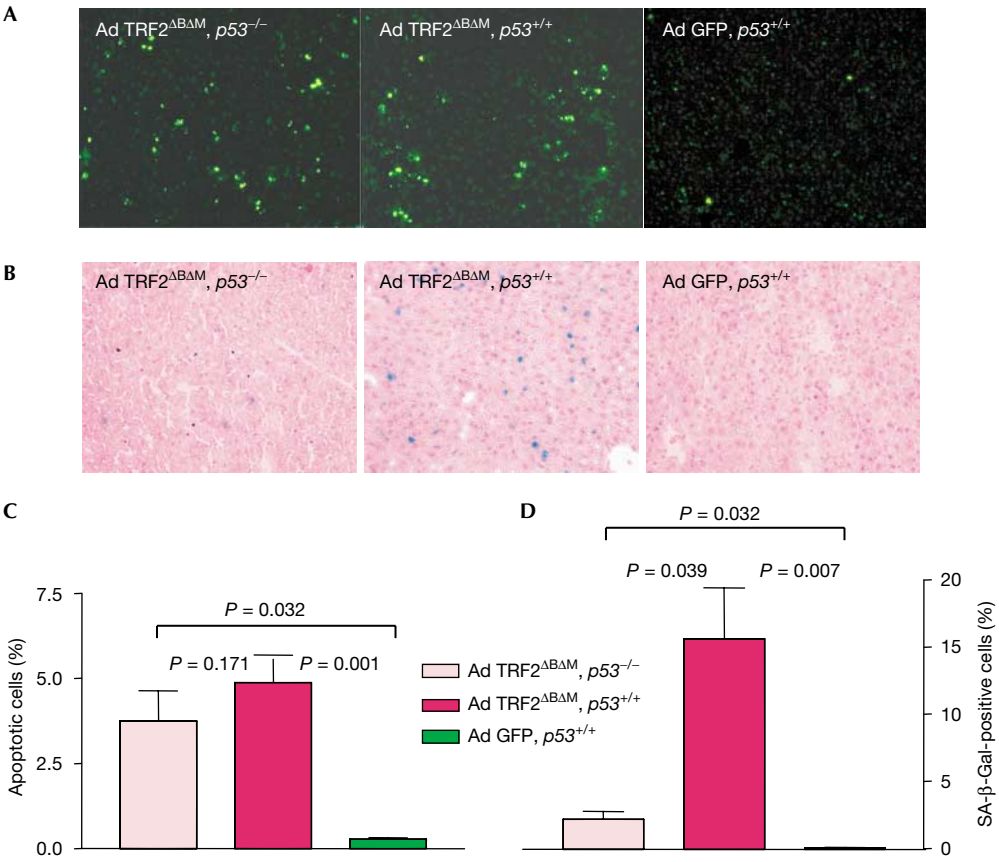

Fig 4 | TRF2$^{\Delta B\Delta M}$ expression induces *p53*-independent apoptosis but *p53*-dependent senescence. The impact of *p53* status on the effects of the loss of telomere protection by Ad TRF2$^{\Delta B\Delta M}$ (1×10^{10} PFU/ml) infection was analysed by comparing *p53* wild-type ($p53^{+/+}$) and *p53*-knockout ($p53^{-/-}$) mice ($n = 5$). (**A**) Representative photographs of TUNEL-positive liver cells 48 h after TRF2$^{\Delta B\Delta M}$ infection in $p53^{-/-}$ mice (left), $p53^{+/+}$ mice (middle) and GFP control-infected $p53^{+/+}$ mice (right) (magnification: $\times 200$). (**B**) Representative photographs of SA-β-Gal-stained liver sections 48 h after Ad TRF2$^{\Delta B\Delta M}$ infection of $p53^{-/-}$ mice (left), Ad TRF2$^{\Delta B\Delta M}$ infection of $p53^{+/+}$ mice (middle) and Ad GFP infection of $p53^{+/+}$ mice (right) (magnification: $\times 200$). (**C**) Percentage of apoptotic liver cells 48 h after Ad TRF2$^{\Delta B\Delta M}$ or Ad GFP infection. Note that the increase in apoptotic cells in Ad TRF2$^{\Delta B\Delta M}$-infected mice is *p53* independent. (**D**) Percentage of SA-β-Gal-positive liver cells 48 h after Ad TRF2$^{\Delta B\Delta M}$ infection. Note that the increase in SA-β-Gal-positive cells in Ad TRF2$^{\Delta B\Delta M}$-infected mice is *p53* dependent.

with a secondary Cy3-labelled rabbit anti-mouse antibody (1:500) for 30 min. The number of apoptotic cells ($n = 400$) in correlation with the level of TRF2$^{\Delta B\Delta M}$ expression was counted in randomly chosen low-power fields ($\times 200$; $n = 4$ mice).

Feulgen staining. Feulgen staining was performed according to standard methods. The intensity of Feulgen staining was analysed with ACAS software (Ahrens Cytometry Analysis System for flow and static cytometry, Bargteheide/Hamburg, Germany). For each sample, 300 hepatocyte nuclei were analysed.

Metaphase spreads. After 48 h of adenovirus infection (Ad TRF2$^{\Delta B\Delta M}$, $n = 3$; Ad GFP, $n = 4$), the mice were treated with colcemid (a total of 20 μg/mouse) by intraperitoneal injection. At 24 h after colcemid injection, the liver cells were collected by liver perfusion as described previously (Satyanarayana *et al*, 2003).

Telomere fluorescence *in situ* hybridization. Quantitative fluorescence *in situ* hybridization (Q-FISH) was carried out as described previously (Plentz *et al*, 2004). Signals were detected using an epifluorescence microscope (Carl Zeiss Jena GmbH, Jena, Germany) equipped with a CCD camera and FISH View software (Applied Spectral Imaging Ltd, Migdal HaEmek, Israel).

FACS analysis. Cells were collected by liver perfusion at different time points and immediately used for TRF2 and TUNEL staining. They were then analysed by FACS Calibur flow cytometer (Becton Dickinson, Franklin Lakes, NJ, USA). The cells were double stained for TRF2 with Cy3-labelled goat anti-mouse antibody (1:100; Zymed) and TUNEL to analyse the apoptosis. For measuring senescence, cells were stained for TRF2 with FITC-labelled goat anti-mouse (1:100; Caltag, Burlingame, CA, USA) and cell size was monitored by forward scatter (FSC). The gating for selection of large-senescent and small non-senescent cells was used as described previously (Gorbunova *et al*, 2003; Martin-Ruiz *et al*, 2004) using Ad GFP-infected and non-infected mice as controls.

Statistical programs. Student's *t*-test, Graphpad Instat, Graphpad Prism and Microsoft Excel software was used to calculate the statistical significance and standard deviations.

Supplementary information is available at *EMBO reports* online (http://www.emboreports.org).

ACKNOWLEDGEMENTS

We thank T. de Lange for providing the Ad TRF2$^{\Delta B\Delta M}$ virus and Dr Hecker for statistical analysis. K.L.R. is supported by the Deutsche Forschungsgemeinschaft (Emmy-Noether-Programm: Ru 745/2-1, Ru745 4-1 and KFO119) and a grant from the Deutsche Krebshilfe e.V. (10-2236-Ru 2).

REFERENCES

Blackburn EH, Chan S, Chang J, Fulton TB, Krauskopf A, McEachern M, Prescott J, Roy J, Smith C, Wang H (2000) Molecular manifestations and molecular determinants of telomere capping. *Cold Spring Harb Symp Quant Biol* **65:** 253–263

Chin L, Artandi SE, Shen Q, Tam A, Lee SL, Gottlieb GJ, Greider CW, DePinho RA (1999) *p53* deficiency rescues the adverse effects of telomere loss and cooperates with telomere dysfunction to accelerate carcinogenesis. *Cell* **97:** 527–538

Cimino-Reale G, Pascale E, Starace G, Verna R, D'Ambrosio E (2001) The length of telomeric G-rich strand 3′-overhang measured by oligonucleotide ligation assay. *Nucleic Acids Res* **29:** E35

d'Adda di Fagagna F, Reaper PM, Clay-Farrace L, Fiegler H, Carr P, Von Zglinicki T, Saretzki G, Carter NP, Jackson SP (2003) A DNA damage checkpoint response in telomere-initiated senescence. *Nature* **13:** 194–198

de Lange T (2002) Protection of mammalian telomeres. *Oncogene* **21:** 532–540

Dimri GP *et al* (1995) A biomarker that identifies senescent human cells in culture and in aging skin *in vivo*. *Proc Natl Acad Sci USA* **92:** 9363–9367

Djojosubroto MW, Choi YS, Lee HW, Rudolph KL (2003) Telomeres and telomerase in aging, regeneration and cancer. *Mol Cells* **15:** 164–175

Gorbunova V, Seluanov A, Pereira-Smith OM (2003) Evidence that high telomerase activity may induce a senescent-like growth arrest in human fibroblasts. *J Biol Chem* **278:** 7692–7698

Karlseder J, Broccoli D, Dai Y, Hardy S, de Lange T (1999) *p53*- and ATM-dependent apoptosis induced by telomeres lacking TRF2. *Science* **283:** 1321–1325

Karlseder J, Smogorzewska A, de Lange T (2002) Senescence induced by altered telomere state, not telomere loss. *Science* **295:** 2446–2449

Keys B, Serra V, Saretzki G, Von Zglinicki T (2004) Telomere shortening in human fibroblasts is not dependent on the size of the telomeric-3′-overhang. *Aging Cell* **3:** 103–109

Krishnamurthy J, Torrice C, Ramsey MR, Kovalev GI, Al-Regaiey K, Su L, Sharpless NE (2004) Arf expression is a biomarker of aging. *J Clin Invest* **114:** 1299–1307

Lee HW, Blasco MA, Gottlieb GJ, Horner II JW, Greider CW, DePinho RA (1998) Essential role of mouse telomerase in highly proliferative organs. *Nature* **392:** 569–574

Martin-Ruiz C, Saretzki G, Petrie J, Ladhoff J, Jeyapalan J, Wei W, Sedivy J, von Zglinicki T (2004) Variation in telomere shortening rate causes heterogeneity of human fibroblast replicative life span. *J Biol Chem* **279:** 17826–17833

Parrinello S, Samper E, Krtolica A, Goldstein J, Melov S, Campisi J (2003) Oxygen sensitivity severely limits the replicative lifespan of murine fibroblasts. *Nat Cell Biol* **5:** 741–747

Plentz RR, Caselitz M, Bleck JS, Gebel M, Flemming P, Kubicka S, Manns MP, Rudolph KL (2004) Hepatocellular telomere shortening correlates with chromosomal instability and the development of human hepatoma. *Hepatology* **40:** 80–86

Rudolph KL, Chang S, Millard M, Schreiber-Agus N, DePinho RA (2000) Inhibition of experimental liver cirrhosis in mice by telomerase gene delivery. *Science* **287:** 1253–1258

Satyanarayana A, Wiemann SU, Buer J, Lauber J, Dittmar KEJ, Wüstefeld T, Blasco M, Manns MP, Rudolph KL (2003) Telomere shortening impairs organ regeneration by inhibiting cell cycle re-entry of a subpopulation of cells. *EMBO J* **22:** 4003–4013

Satyanarayana A, Greenberg RA, Schaetzlein S, Buer J, Masutomi K, Hahn WC, Zimmermann S, Martens U, Manns MP, Rudolph KL (2004a) Mitogen stimulation cooperates with telomere shortening to activate DNA damage responses and senescence signaling. *Mol Cell Biol* **24:** 5459–5474

Satyanarayana A, Manns MP, Rudolph KL (2004b) Telomeres and telomerase: a dual role in hepatocarcinogenesis. *Hepatology* **40:** 276–283

Shay JW, Pereira-Smith OM, Wright WE (1991) A role for both RB and *p53* in the regulation of human cellular senescence. *Exp Cell Res* **96:** 1–6

Smogorzewska A, de Lange T (2002) Different telomere damage signaling pathways in human and mouse cells. *EMBO J* **21:** 4338–4348

van Steensel B, Smogorzewska A, de Lange T (1998) TRF2 protects human telomeres from end-to-end fusions. *Cell* **92:** 401–413